Formation of magnetic filaments: A kinetic study

F. Martínez-Pedrero, M. Tirado-Miranda, A. Schmitt, and J. Callejas-Fernández*
Department of Applied Physics, University of Granada, Campus de Fuentenueva, E-18071 Granada, Spain
(Received 9 April 2007; revised manuscript received 21 May 2007; published 18 July 2007)

In order to form magnetic filaments or chains, aqueous suspensions of superparamagnetic colloidal particles were aggregated under the action of an external magnetic field in the presence of different amounts of an indifferent 1:1 electrolyte (KBr). This allowed the influence of the anisotropic magnetic and isotropic electrostatic interactions on the aggregation behavior of these electric double-layered magnetic particles to be studied. Dynamic light scattering was used for monitoring the average diffusion coefficient of the magnetic filaments formed. Hydrodynamic equations were employed for obtaining the average chain lengths from the experimental mean diffusion coefficients. The results show that, for the same exposure time to the magnetic field, the average filament size is monotonously related to the amount of electrolyte added. The chain growth behavior was found to follow a power law with a similar exponent for all electrolyte concentrations used in this work. The time evolution of the average filament size can be rescaled such that all the curves collapse on a single master curve. Since the electrolyte added does not have any effect on the scaling behavior, the mechanism of aggregation seems to be completely controlled by the dipolar interaction. However, electrolyte addition not only controls the range of the total interaction between the particles, but also enhances the growth rate of the aggregation process. Taking into account the anisotropic character of these aggregation processes we propose a kernel that depends explicitly on the range of the dipolar interaction. The corresponding solutions of the Smoluchowski equation combined with theoretical models for the diffusion and light scattering by rigid rods reproduce the measured time evolution of the average perpendicular aggregate diffusion coefficient quite satisfactorily.

DOI: 10.1103/PhysRevE.76.011405 PACS number(s): 82.70.Dd, 61.43.Hv, 47.65.Cb

I. INTRODUCTION

Magnetorheological fluids are dispersions of colloidal particles that present an anisotropic interaction when exposed to an external magnetic field, i.e., the particles experience an attractive force along the field direction and a repulsive force normal to it. The intensity of the magnetic interaction is tuneable through the strength of the applied magnetic field. When the particles are allowed to aggregate, linear structures are formed [1]. These magnetic filaments (MF) are able to survive in the absence of the applied field when the chain forming particles are linked by other sufficiently strong nonmagnetic adhesive forces [2]. For a variety of technological applications an adequate modelling of the chain formation process turns out to be of practical importance (see Refs. [3,4] and references therein).

Moreover, when the particles are suspended in aqueous media they usually bear a nonvanishing net surface charge that gives rise to isotropic electrostatic interactions. The interplay between these isotropic electrostatic and the anisotropic magnetic interactions is of interest not only from an applied but also from a theoretical point of view. A challenging and quite difficult task is, e.g., to achieve a reliable control of the final size of the MF by tuning the different interparticle interactions directly. So far, most of the research works dealing with magnetic colloidal particles only consider magnetic forces. Nevertheless, further interactions such as London–van der Waals and electrostatic forces play also an important role and should, as we will show, not be neglected.

A large number of presentations regarding the aggregation behavior of magnetic colloids in three dimensions address the rheological properties of the aggregated samples. Only a few works focus also on a detailed analysis of the chain formation process [5–10]. In their pioneer work, Promislow and Gast determined the mean cluster size as a function of the exposure time to the magnetic field by means of optical microscopy [5]. They found a power-law time dependency that was in good agreement with the theoretical predictions made by Miyazima *et al.* for aggregation of oriented anisotropic particles [6]. Several papers presented since then report a variety of values for the kinetic exponent at different field strengths and particle volume fractions [5,7]. Even alternative theoretical dependencies were proposed [8,9]. Only Miyazima *et al.* proposed an analytical kernel capable to predict the observed power-law dependency for the time evolution of the average cluster size [10]. Their aggregation kernel assumes that the cross section of a chainlike aggregate should not depend on its total length. Nevertheless, it does not consider other important parameters such as the diffusion coefficient of the chains and the range of the interactions. Hence, the kinetics of magnetic chain formation processes is still not completely understood and remains an open question. One of the steps would be to improve the theoretical description proposing an aggregation kernel that includes those physical parameters explicitly. The corresponding solutions of the Smoluchowski equation would then allow, e.g., the time evolution of the average cluster size to be predicted more reliably.

The aim of this work is twofold: (a) to deepen our knowledge about chain formation processes and to study the influence of the interplay between isotropic electric and anisotropic magnetic colloidal interactions; (b) to derive an

*jcalleja@ugr.es

aggregation kernel for an improved theoretical description of the experimental results. This aggregation kernel considers an effective aggregation cross section and depends explicitly on the average range of the interactions. The results will show that electrostatic repulsions control the aggregation kinetics and thus, also play an important role in field induced aggregation processes. The aggregation mechanism and cluster structure, however, will be mainly governed by the anisotropic magnetic interaction.

The outline of this paper is as follows: The next section gives a description of the theoretical background needed for this study. The materials and methods are described in Sec. III. Sections IV and V present results and conclusions, respectively.

II. THEORETICAL BACKGROUND

The theoretical analysis used in this work is based on the assumption that chains of magnetic particles may be modelled as rigid cylinders of length L and diameter $d=2a$, where a is the particle radius. Then, theoretical models for rigid rods undergoing translational and rotational Brownian motion may be used for describing filament diffusion. The Maeda and Fujime model has shown to be a useful tool for this purpose [11,12]. Nevertheless, the presence of an external magnetic field introduces a preferential orientation in space and impedes the rotational diffusion of the chains. Hence, modelling the chains as cylinders, their average translational diffusion coefficient may be expressed as $\bar{D}=\frac{1}{3}D_{\parallel}+\frac{2}{3}D_{\perp}$, where $D_{\parallel}$ and $D_{\perp}$ are the translational diffusion coefficients parallel and perpendicular to the longer axis of the rods, respectively [11]. Tirado *et al.* proposed

$$D_{\parallel}=\frac{k_BT}{2\pi\eta L}\left[\ln\left(\frac{L}{d}\right)+\gamma_{\parallel}(L)\right], \tag{2.1a}$$

$$D_{\perp}=\frac{k_BT}{4\pi\eta L}\left[\ln\left(\frac{L}{d}\right)+\gamma_{\perp}(L)\right], \tag{2.1b}$$

for the relationship between these diffusion coefficients and the chain length [13]. Here, η is the solvent viscosity and k_BT is the thermal energy. The cylinder length functions $\gamma_{\parallel}(L)$ and $\gamma_{\perp}(L)$ account for the so-called end-of-chain effects. They may be written as $\gamma_{\parallel}=-0.21+\frac{0.90}{N}$ and $\gamma_{\perp}=0.84+\frac{0.18}{N}+\frac{0.24}{N^2}$, where $N=\frac{L}{d}$ is the number of particles per aggregate.

According to the current light scattering theory, the average diffusion coefficient $\langle D(q,t)\rangle$ measured by dynamic light scattering (DLS) is related to the diffusion coefficients of the different clusters of size N through the expression

$$\langle D(q,t)\rangle=\frac{\sum_{N=1}^{N_c}n_N(t)N^2S(qR_g)D(N)}{\sum_{N=1}^{N_c}n_N(t)N^2S(qR_g)}, \tag{2.2}$$

where $n_N(t)$ is the cluster size distribution, $S(qR_g)$ is the structure factor that accounts for the spatial distribution of the individual particles within the aggregates, and $D(N)$ is the diffusion coefficient of a cluster formed by N monomeric particles [14,15]. The cutoff size N_c is the size of the largest aggregate in the system. R_g is the aggregate radius of gyration and $q=\frac{4\pi}{\lambda_m}\sin\left(\frac{\theta}{2}\right)$ is the scattering vector. Here, θ is the scattering angle and λ_m is the wavelength in the dispersion medium.

In the literature, several functional forms for the structure factor of spherical but not of linear aggregates can be found [14–16]. Hence, we replaced $S(qR_g)$ by the form factor of linear cylinders that is given by

$$S(u)=\left|\frac{2}{u}J_1(u)\right|^2, \tag{2.3}$$

where $u=2qa\sin\left(\frac{\theta}{2}\right)\sin\beta$, and β is the angle between the longer cylinder axis and the scattering plane [17].

The time evolution of the cluster size distribution $n_N(t)$ in aggregating systems may be modelled by solving Smoluchowski's rate equation [18]. This mean-field-type equation is

$$\frac{dn_N}{dt}=\frac{1}{2}\sum_{i+j=N}k_{ij}n_in_j-\sum_{N=1}^{\infty}k_{iN}n_i. \tag{2.4}$$

It is frequently employed for describing aggregation processes arising in diluted samples. Here, k_{ij} is the aggregation kernel which must be understood as an orientational and configurational average of the exact aggregation rates for two specific clusters of size i and j that collide under a particular orientation.

For pure diffusion-limited aggregation, the so-called *Brownian kernel* (BK),

$$k_{ij}=4\pi(a_i+a_j)(D_i+D_j), \tag{2.5}$$

is known to describe the corresponding aggregation kinetics quite satisfactorily. The BK is strictly valid only for solid spheres of radius a_i and a_j that undergo isotropic Brownian motion and aggregate as soon as they come into contact, i.e., when the distance between their centers becomes a_i+a_j [19]. It was derived considering a system of particles of size i that diffuse freely in the presence of another particle of size j placed at the origin of the coordinate system. The latter particle is acting as a sink since all the particles of radius a_i that come into contact with it will form aggregates of size $i+j$. Hence, there are no individual particles of radius a_i at the contact surface and the corresponding boundary condition becomes $c_i(r=a_i+a_j,t)=0$, where $c_i(r,t)$ is the concentration of particles of size i, the distance r points from the center of the sink particle to the centers of the diffusing spheres. Solving the diffusion equation for this configuration, the radial particle flux density $j_r(r,t)$ may be determined. The number of particles of radius a_i that aggregate with the sink particle $J_r(t)$ is simply the number of particles that diffuse towards the sink particle and get in contact with it. Evidently, this number can be obtained by multiplying the radial flux density with the area of the contact surface, i.e., with $4\pi(a_i+a_j)^2$. This yields

$$J_r(t) = 4\pi(a_i + a_j)^2 j_r(r,t) = -4\pi(a_i + a_j)D_{ij}\left(1 + \frac{a_i + a_j}{\sqrt{\pi D_{ij} t}}\right)c_i, \tag{2.6}$$

where $j_r(r=a_i+a_j,t)=-D_{ij}c_i\left(\frac{1}{a_i+a_j}+\frac{1}{\sqrt{\pi D_{ij}t}}\right)$ is the radial particle flux density at the contact surface, $D_{ij}=D_i+D_j$ is the relative diffusion coefficient, and c_i is the bulk concentration of the particles of size i. For colloidal aggregation in three dimensions, the steady state is reached very fast and so, the time-dependent term is usually neglected. Multiplying net particle flux $J_r(t)$ for one central particle by the concentration of sink particles c_j gives the total number of particles of size i that aggregate per unit time and unit volume. The result obtained is the following:

$$\frac{dc_i}{dt} = J_r(t)c_j = -4\pi(a_i + a_j)(D_i + D_j)c_i c_j = -k_{ij}c_i c_j. \tag{2.7}$$

This expression has the typical form of a kinetic rate equation with an aggregation rate constant k_{ij} given by the BK [Eq. (2.5)].

Several authors suggested that a kernel for aggregation of magnetic particle dispersions should be based on the BK. In fact, Miyazima *et al.* used the BK for describing the time evolution of the average cluster size arising in aggregating dispersions of dipolar particles aligned under the influence of an external field. They assumed the linear aggregates of dipolar particles at not too high concentrations to behave as rodlike clusters that aggregate tip to tip. Supposing the chain ends to be the only active aggregation sites, they conclude that the collision cross section and the corresponding term in the BK should be constant. The cluster diffusion coefficients, however, were considered to depend on the cluster size as a power law, i.e., as $D \propto i^{\gamma}$. Based on these assumptions, they proposed the following power-law-type aggregation kernel:

$$k_{ij} \propto (i^{\gamma} + j^{\gamma}). \tag{2.8}$$

This kernel is a homogeneous function of the cluster size i and j, being γ the corresponding homogeneity exponent. For such kernels, dynamical scaling theory predicts the average cluster size to diverge as power of time, i.e., as $N(t) \propto t^z$. The kinetic exponent z is directly related to the homogeneity exponent through the expression $z=\frac{1}{1-\gamma}$ [6].

It should be noted that the kernel proposed by Miyazima *et al.* implicitly accepted the hypothesis of isotropic diffusion and spherical symmetry that was used for deriving the BK. During field induced aggregation processes, however, spherical symmetry is lost and the cluster diffusion ceases to be isotropic. Moreover, the net interaction between two approaching chains becomes long ranged and may be either attractive or repulsive. All theses effects are not accounted for in the Miyazima kernel. Hence, it is not clear at all why this kernel should be employed for describing the aggregation behavior of magnetic chains. In what follows, we will use physical yet somewhat heuristic arguments for deriving a kernel for field induced aggregation that considers not only the long-range character but also the anisotropic nature of the magnetic dipole-dipole interactions among the particles.

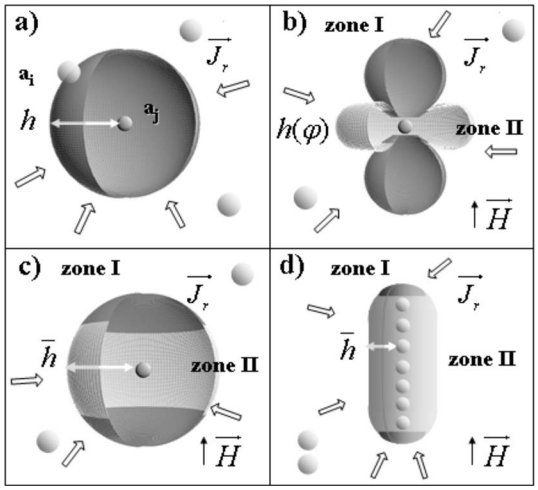

FIG. 1. Schematic illustrations of the space around the sink particles considered for deriving an aggregation kernel for the field induced aggregation. In the plots, the attractive and repulsive regions are indicated as zones I and II, respectively. The arrows symbolize the radial flux of i size particles towards the sink particle.

For this purpose, we consider the same configuration that was used for deriving the BK, i.e., freely diffusing particles of radius a_i that aggregate as soon as they come into contact with a sink particle of radius a_j. In order to include the long-range character of the net interaction among the approaching particles, we define an effective interaction range h such that the particles will, on average, aggregate as soon as the distance between the particle surfaces becomes smaller than h. This means that the sink particle behaves as if it were a sphere with an effective radius of a_j+h [see Fig. 1(a)]. Modifying the BK accordingly yields

$$k_{ij} = 4\pi(a_i + a_j + h)(D_i + D_j). \tag{2.9}$$

For interacting magnetic particles, however, the interaction may be either attractive or repulsive and its range depends on the angle φ between the external magnetic field and the line joining the particle centers. According to magnetic theory, the interaction range $h(\varphi)$ is proportional to $\sqrt[3]{|3\cos^2\varphi - 1|}$ [5]. Figure 1(b) shows a three-dimensional plot of $h(\varphi)$. In the figure, the attractive and repulsive regions are indicated as zones I and II, respectively. As can be seen, the attractive region has a dumbbell-like shape and fits in a symmetric double cone with an aperture angle of $\varphi_c = 54.7356 \approx 55°$ with respect to the field direction. Evidently, all the particles flowing into the dumbbell-shaped attractive region will aggregate while those trying to enter zone II will be repelled. The corresponding aggregation kernel could, in principle, be derived by solving the diffusion equation for this configuration.

Due to the missing spherical symmetry, however, this is not straightforward. Hence, we propose to simplify the problem somewhat further and to consider an angle independent effective interaction range $\bar{h}$ maintaining the aperture angle

of the attractive zone [see Fig. 1(c)]. This means that the particles of radius a_i will be diffusing freely until the center-to-center distance to the sink particle becomes $a_i+\bar{h}+a_j$. Hence, the spherical shape of the contact surface is recovered and the sink particle will again behave as a sphere with an effective radius of $a_j+\bar{h}$. Evidently, only the particles diffusing through the attractive pole caps of the effective spherical contact surface will aggregate while the particles approaching the lateral regions will be repelled. Hence, only the fraction $A_{pc}/A_0=(1-\cos\varphi_c)$ of the total flux of particles towards the sink particle will be effective. Here, A_{pc} is the total area of the pole caps while A_0 is the area of the entire sphere. Based on these approximations, the corresponding aggregation kernel becomes

$$k_{ij}=4\pi(1-\cos\varphi_c)(a_i+a_j+\bar{h})(D_i+D_j). \qquad (2.10)$$

This aggregation kernel should provide a reasonable description for the aggregation behavior of spherical particles of radii a_i and a_j that interact like aligned magnetic dipoles.

The final step is to extend the validity of the kernel given by Eq. (2.10) to the field-induced aggregation processes where chainlike clusters are formed. Figure 1(d) shows a schematic view of a chainlike aggregate consisting of aligned magnetic particles of identical radius a. At not too high concentrations, laterally approaching particles or chainlike clusters are repelled while those arriving at the chain ends will be attracted. In other words, there is an attractive zone at the chain tips and a repulsive region at the lateral chain side. If one accepts that the effective range $\bar{h}$ of the net magnetic interaction and the aperture angle of the attractive zone are not affected too much by the presence of further chain-forming particles, then the area of the attractive zone at the chain tips will be approximately the same as the one of individual particles. Consequently, the net flux of clusters that diffuse through that surface and aggregate with the cluster must also be very similar. This means that the kernel derived for individual particles [Eq. (2.10)] should also be able to describe the aggregation behavior of chainlike aggregates if also the diffusion behavior of the chains were not affected by the presence of further particles in the chain. The latter is, of course, not the case and so, we propose to replace the diffusion coefficients in the aggregation kernel by the average translational diffusion coefficient $\bar{D}$ of rods mentioned at the beginning of the theory section. Based on these assumptions, the kernel for field induced aggregation processes arising in magnetic particle dispersions becomes

$$k_{ij}=4\pi(1-\cos\varphi_c)(2a+\bar{h})(\bar{D}_i+\bar{D}_j), \qquad (2.11)$$

This aggregation kernel should be understood as a heuristic mean-field approximation using effective quantities such as the effective interaction range $\bar{h}$ and the effective diffusion coefficients $\bar{D}_i$ and $\bar{D}_j$. It should be noted that the only freely adjustable parameter is the effective interaction range $\bar{h}$. Equation (2.11) is an analytical expression for an aggregation kernel for the field induced aggregation processes that is explicitly expressed in terms of physically meaningful quantities.

III. MATERIALS AND METHODS

A. Materials

The magnetic latex particles used in this work were purchased from Merck Laboratories. The particles are roughly monodisperse polystyrene spheres with an average diameter of (170±5) nm. Their magnetic character derives from magnetite grains of approximately 10 nm in size that are randomly distributed within the polystyrene matrix. Magnetization curves reveal the superparamagnetic character of these beads, i.e., there is no remanent magnetization that is characteristic for ferromagnetic materials and their magnetic response is at least four orders of magnitude stronger than the one of typical paramagnetic materials. Consequently, dipolar magnetic interactions between those particles only appear in the presence of an applied magnetic field. The particles are dispersed in water. The stability of the system is ensured by repulsive forces due to superficial carboxylic groups and anionic sodium dodecyl sulphate SDS surfactant molecules absorbed on the particle surface. The particle surface potential of −50 mV was obtained by means of electrophoretic mobility measurements. Due to their relatively low density of 1.2 g/cm^3, particle sedimentation was found to be negligible during the experiments. According to the manufacturer, the magnetic polystyrene particles have a ferrite mass content of 53.2% and a saturation magnetization M_s of approximately 36 kA/m. The particles reach the saturation magnetization for applied magnetic fields stronger than 70 mT.

B. Methods

Several series of experiments have been performed at different concentrations of an indifferent 1:1 electrolyte (KBr). The final electrolyte concentrations used for reducing the repulsive electrostatic interactions ranged from 0 mM to 50 mM. Up to an electrolyte concentration of approximately 50 mM, the systems remained stable when they were not exposed to the magnetic field [12]. Prior to the aggregation experiments, the diluted samples were filtered through a 450 nm pore size membrane filter in order to eliminate primary clusters.

The electrolyte was always added to the colloidal dispersion before exposing the samples to the magnetic field. This was achieved by mixing equal amounts of KBr solution and particle suspension through a Y-shaped mixing device directly into the measuring cell. Afterwards, the magnetic field was applied by placing several magnetic disks on the top and on the bottom of the measurement cell. The magnetic field strength was measured to be $H=23.9$ kA/m throughout the scattering volume. The divergence of the applied magnetic field was small enough so that significant particle migration was not observed during the experiments.

The light scattering experiments were performed using a Malvern 4700C instrument working with a vertically polarized 632.8 nm wavelength HeNe laser. The particle number concentration was always adjusted to $1.0\times10^{10}\frac{1}{cm^3}$, corresponding to a volume fraction of $\phi=2.6\times10^{-5}$. The low particle concentration avoids multiple light scattering and lateral chain-chain aggregation. The DLS measurements

were always performed at a scattering angle of $\theta=60°$ ($q^{-1}=75.7$ nm). Data analysis was carried out using software developed by our team. The effective diffusion coefficient $\langle D(q,t)\rangle$ was obtained from the first cumulant $\mu_1 = \langle D(q,t)\rangle q^2$ of the intensity autocorrelation function.

The geometry of the experiment deserves a detailed comment. The external magnetic field was applied perpendicularly to the scattering plane, and the filaments are forced to align in the same direction. Hence, the measurements are only sensitive to transversal motion perpendicular to the chains axis. These facts have two important consequences. On the one hand, $S(q)$ may be approximated by the structure factor of cylindrical rods with their axis aligned perpendicular to the scattering plane, i.e., it is sufficient to consider $\beta = \frac{\pi}{2}$ in Eq. (2.3). On the other hand, rotational chain diffusion is not possible when the field is applied. Consequently, only the translational diffusion coefficient perpendicular to the rod axis $D_\perp$ must be considered when Eq. (2.2) is used.

Moreover, linear aggregates of magnetic particles may also bend and twist slightly due to Brownian motion. Such internal fluctuations may give rise to an additional contribution to the measured average diffusion coefficient. Using surfactant coated kerosene-based ferrofluid droplet particles, Cutillas *et al.* have shown experimentally that such positional fluctuations of the particles within the chains cause a linear dependency of the mean diffusion coefficient on q [20]. Their experiments also verified that the chains become more rigid and the fluctuations disappear as the field strength increases. In close analogy with polymer chain dynamics, they were able to describe the q dependency of the mean diffusion coefficient $\langle D(q,t)\rangle$ for their experimental system by the following empiric linear approximation:

$$\langle D(q,t)\rangle \approx \left(\frac{2}{\sqrt{\lambda}}qa+1\right)D_\perp. \tag{3.1}$$

The slope in this relationship depends on the magnetic field strength through the dimensionless parameter $\lambda=\frac{\pi\mu_0 a^3\chi^2H^2}{9k_BT}$ which represents the ratio between the maximum attractive magnetic dipole-dipole energy and the thermal energy. Here, μ_0 is the permeability of free space, χ is the magnetic susceptibility, and H is the external field strength [5]. From magnetization curves, we estimated the susceptibility of our particles to be $\chi\approx 0.59$ at the external magnetic field strength used for the experiments. This leads to $\lambda\approx 118$ and means that the magnetic field may already be strong enough to avoid significant internal chain fluctuations. In order to check this hypothesis, we measured the diffusion coefficient as a function of q. Since no q dependency was found, we conclude that our chains behave like rigid rods without any significant internal motion. Hence, we may safely assume the effective diffusion coefficient measured by DLS to contain only a contribution due to perpendicular translational chain diffusion.

The time evolution of the cluster size distributions $n_N(t)$ were obtained using the stochastic method described in Ref. [21]. For this purpose, the kernels k_{ij} proposed in the theory section [Eq. (2.11) and Eq. (2.8)] were considered. In all cases, monomeric initial conditions $n_N(t=0)=n_0\delta_{1N}$ were imposed. Here, n_0 is the initial particle concentration and δ_{1N} is the well-known Kronecker symbol.

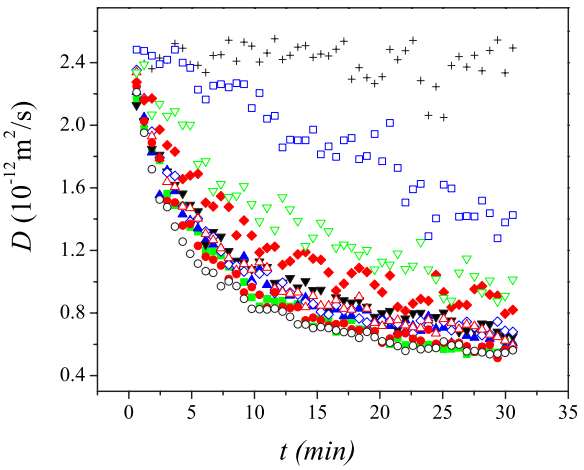

FIG. 2. (Color online) Effective diffusion coefficient of the aggregated samples versus exposure time to the applied magnetic field. The electrolyte concentrations in the samples were (+) 0.0 mM, (□) 0.10 mM, (▽) 0.25 mM, (◆) 0.50 mM, (△) 1.0 mM, (◇) 2.0 mM, (▼) 5.0 mM, (▲) 10 mM, (■) 20 mM, (●) 25 mM, and (○) 50 mM KBr.

IV. RESULTS

Figure 2 shows the measured effective aggregate diffusion coefficient $\langle D(q,t)\rangle$ as a function of the exposure time to the applied magnetic field for all electrolyte concentrations used in this study. The data are the average of at least five measurements that were carried out. The corresponding error bars are not shown for the sake of clarity. Excluding the electrolyte free sample, a decrease of $\langle D(q,t)\rangle$ is observed in all cases. This means that the average filament size increases with the exposure time to the magnetic field. Aggregation is not observed for the electrolyte free sample. For increasing electrolyte concentrations, the growth rate rises and reaches a limiting value already at about 50 mM KBr. This shows clearly that the electrostatic repulsion between the particles at lower electrolyte concentrations is strong enough to slow down aggregation at least partially. At high electrolyte concentration, however, the electrostatic repulsion is overcome completely by the magnetic interaction. For the higher electrolyte concentrations, the results superimpose and follow the curve observed at 50 mM.

From the data for the perpendicular diffusion coefficient, the average chain length, expressed in number of particles per aggregate N, was extracted according to the hydrodynamic equation [Eq. (2.1b)] proposed by Tirado *et al.* The obtained results are shown in Fig. 3 in logarithmic scale only for the most representative cases, i.e., at electrolyte concentrations of 0.10, 0.25, 1.0, and 50 mM. It should be noted that chain formation takes place even at relatively low electrolyte concentrations. These electrolyte concentrations are too low to affect the stability of the samples when the magnetic field is absent. Once the field is applied, however, linear

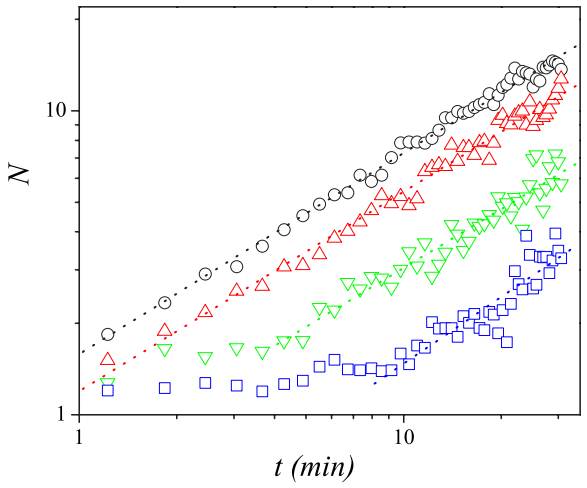

FIG. 3. (Color online) Average number of constituent particles per aggregate as a function of the exposure time to the external magnetic field at electrolyte concentrations of (□) 0.10 mM, (▽) 0.25 mM, (△) 1.0 mM, and (○) 50 mM. The dotted straight lines show asymptotic behavior according to $N \propto t^z$.

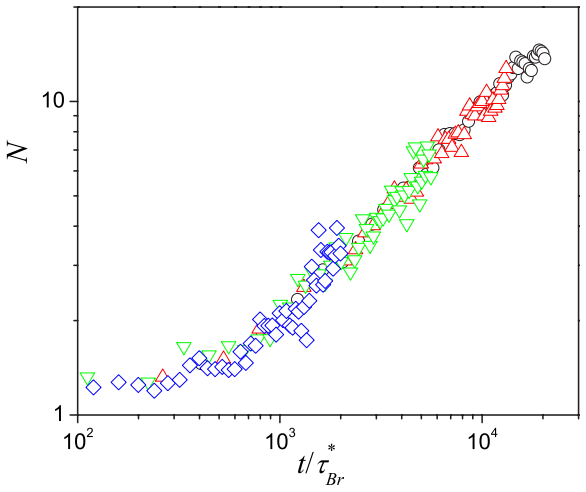

FIG. 4. (Color online) Average number of constituent particles per aggregate as a function of the scaled exposure time at electrolyte concentrations of (□) 0.10 mM, (▽) 0.25 mM, (△) 1.0 mM, and (○) 50 mM.

aggregates start to grow. The growth behavior depends strongly on small variations of the electrolyte concentration. Moreover, such low electrolyte concentrations play, as we have observed in a previous work [12], also a fundamental role for the reversibility of the process, once the magnetic field is removed.

According to Fig. 3, the data show a similar asymptotic behavior and follow well-defined straight lines with a slope of $z=0.67\pm0.04$ for all the electrolyte concentrations used. Such a power-law dependence has been reported by most of the experimental and numerical studies. The measured kinetic exponent is similar to the values obtained in the literature. For magnetic field induced aggregation, Promislow *et al.* reported values ranging from 0.50 to 0.75 depending on the volume fraction. Fraden *et al.* measured $z=0.6$ for the aggregation of dipolar dielectric particles under action of an electric field [5,10]. All these values are close to the value $z=0.5$ obtained by Miyazima using simulations. This value for field induced aggregation was determined neglecting not only the anisotropic character of chain diffusion but also the long-range character of the dipolar interactions [6].

The similarity in shape and the almost identical kinetic exponents of the curves shown in Fig. 3 indicate that the underlying aggregation mechanism does not depend on the electrolyte concentration. Electrolyte addition screens the electrostatic repulsion and so, increases the effective range of the total interaction. This gives rise to an enhanced filament growth rate, i.e., to an increased aggregation rate. Nevertheless, the kinetic exponent does not depend on the electrolyte concentration. This indicates that the aggregation mechanism is controlled by the dipolar magnetic interaction rather than the electrostatic interactions.

Neglecting electrostatic interactions, Promislow *et al.* found the time evolution of the average chain length in pure field induced aggregation processes to collapse on a single master curve when the time axis is rescaled using the characteristic time [5]:

$$\tau_{\mathrm{Br}}^{*} = \frac{a^2}{D_0 \phi_{\mathrm{eff}}} \tag{4.1}$$

where $D_0=\frac{k_B T}{6\pi\eta a}$ is the monomer diffusion coefficient. From a physical point of view, this characteristic time may be interpreted as a modified Brownian time scale that accounts for the attractive nature of the magnetic interaction in terms of an effective particle volume fraction given by $\phi_{\mathrm{eff}} = 24\left[\left(\frac{1}{3}\right)^{1/2} - \left(\frac{1}{3}\right)^{3/2}\right]\lambda\phi$. In other words, the capture volume of the aggregates scales as $a^3\lambda$ due to the long range character of the magnetic interaction.

In our experimental systems, however, electrostatic interactions are present at almost all the electrolyte concentrations employed although the strength of the external magnetic field and consequently λ remain constant. Since similar kinetic exponents were obtained for all the curves shown in Fig. 3, it should be possible to use scaling methods also in our case. Therefore, a characteristic scaling time for the average cluster size must be found. This scaling time should take into account that the effective capture volume is sensitive to both, the electrostatic and the magnetic interactions. Hence, we redefine the effective volume $\phi_{\mathrm{eff}} = 24\left[\left(\frac{1}{3}\right)^{1/2} - \left(\frac{1}{3}\right)^{3/2}\right]\Gamma_{\mathrm{el}}\lambda\phi$ so that it accounts for the effect of the electrostatic interactions through a dimensionless parameter Γ_{el}. This coefficient reflects the influence of the electrolyte concentration on the range of the total interaction and is used here as a freely adjustable fitting parameter for making the data superimpose. In our experimental systems, the repulsive electrostatic interaction is already sufficiently screened and negligible with respect to the magnetic forces at 50 mM. Therefore we assume $\Gamma_{\mathrm{el}}=1$ at this electrolyte concentration and take the 50 mM curve as reference curve onto which the rest of the curves should collapse. Figure 4 shows the average chain length as a function of the scaled time $\frac{t}{\tau_{\mathrm{Br}}^{*}}$ at all the electrolyte concentrations employed. As can be seen, the experimental data align almost perfectly along a single master

TABLE I. The dimensionless parameter Γ_{el}, the effective interaction range $\bar{h}$, and the cross-sectional parameter C assessed for different electrolyte concentrations.

[KBr] (mM)	50	1.0	0.25	0.10
Γ_{el}	1.00	0.66	0.28	0.10
$\frac{\bar{h}}{a}$	3.78	2.72	0.85	−0.42
C ($m^3\ s^{-1}$)	2.34×10^{-17}	1.23×10^{-17}	0.49×10^{-17}	0.15×10^{-17}

curve. The values obtained for Γ_{el} are summarized in Table I. As expected, Γ_{el} decreases for decreasing electrolyte concentration, i.e., it becomes smaller as the electrostatic repulsions become stronger.

Figure 5 shows the time evolution of the measured effective diffusion coefficients in presence of the applied magnetic field. The time is scaled by the characteristic aggregation time for purely diffusion controlled aggregation $t_{agg}=\frac{2}{n_0 k_s}$, where $k_s=12.3\times10^{-18}\ m^3\ s^{-1}$ is Smoluchowski's kinetic rate constant [19]. Time scaling makes it possible to compare the experimental results with theoretical predictions. The continuous lines show the fits that were obtained using the proposed kernel [Eq. (2.11)] for the numerical solutions of Smoluchowski's aggregation equation. In this case, the effective interaction range $\bar{h}$ was the only adjustable parameter. The agreement between experiment and theory can be considered as very satisfying. The values obtained for the fitting parameter $\bar{h}$ are also included in Table I. The effective interaction range and also the effective particle volume fraction increase for increasing electrolyte concentration. These

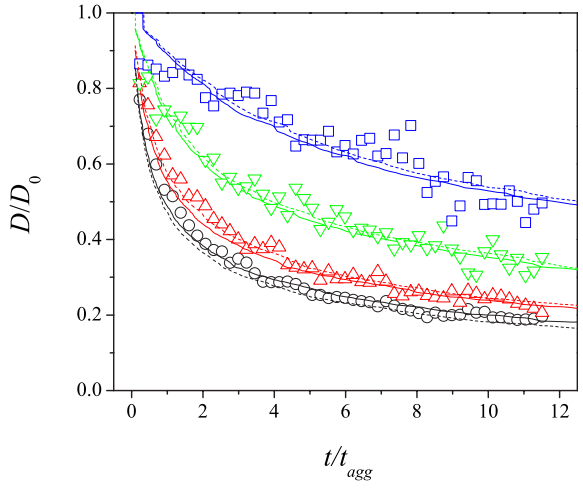

FIG. 5. (Color online) Time dependence of the normalized average diffusion coefficient $\langle D\rangle/D_0$, obtained for electrolyte concentrations of (□) 0.10 mM, (▽) 0.25 mM, (△) 1.0 mM, and (○) 50 mM. The continuous lines show the best fits using the proposed kernel [Eq. (2.11)] for the numerical solutions of Smoluchowski's aggregation equation. The dotted lines show the best fits using the Miyazima kernel [Eq. (2.8)] for the numerical solutions of Smoluchowski's aggregation equation.

observations may be understood in terms of the enhanced shielding of the repulsive electrostatic interaction caused by the electrolyte added. Since the total interaction potential between double-layered magnetic particles usually shows a primary minimum due to strong short-range attractive interactions and a shallow secondary minimum that is mainly due to the long-range magnetic interactions, electrolyte addition plays two important roles for linear aggregate formation. First, it increases the effective range of the total interaction and second, it lowers the height of the energy barrier between both minima [12]. The latter will eventually allow the particles to aggregate in the primary minimum. Only particle-particle bonds in the primary energy minimum are able to persist when the magnetic field is removed. Hence, the relative strength of the electrostatic and magnetic interactions is a fundamental parameter which controls not only the kinetics of chain growth but also their stability once the magnetic field is turned off.

As stated in the theory section, the fitting parameter $\bar{h}$ must be understood as an effective range of net interaction between the aggregates. The real interaction range, however, depends on the angle between the magnetic field direction and the vector indicating the relative position of the interacting species. Moreover, the electrostatic repulsion also modifies the effective interaction range especially at low electrolyte concentrations. The average character of the fitting parameter $\bar{h}$ explains the negative value obtained for the lowest electrolyte concentration of 0.10 mM. At this electrolyte concentration, most of the angular configurations even within the theoretically attractive zone I are in fact repulsive due to the almost unshielded electrostatic interaction.

The experimental results shown in Fig. 3 can also be used to determine the experimental conditions, i.e., the electrolyte concentration and exposure time to the external magnetic field, under which permanent magnetic particle chains of a given average size can be obtained. In other words, the filament size can be controlled by tuning the electrostatic and magnetic interactions accordingly. Maybe it is still too pretentious to talk about "size control" when only a certain average size is achievable. Nevertheless, it is still a first step that may, in a not too far future, lead to a controlled assembly of magnetic filaments. The goal would be to improve the experimental protocol and conditions such that the size distribution is narrowed around the desired mean filament size.

For the sake of completeness, we would like to compare the fits reported above using the proposed kernel [Eq. (2.11)]

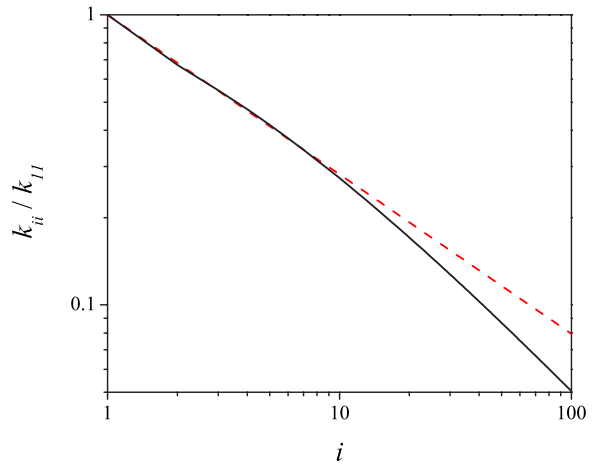

FIG. 6. (Color online) Size dependence of the normalized aggregation rate constant k_{ii} for the proposed kernel (solid line) and the Miyazima kernel with $\gamma=-0.5$ (dashed line).

with fits that could be achieved employing the Miyazima kernel given by $k_{ij}=C(i^{\gamma}+j^{\gamma})$. Therefore, we determined the homogeneity exponent $\gamma=-0.5$ from the experimental kinetic exponent $z=0.67$ and used the proportionality constant C as fitting parameter. The fitting constants obtained are shown in Table I and the corresponding fits are included in Fig. 5. At first sight, the comparable quality of both fits is quite striking. In order to understand the reason thereof, we plotted the normalized rate constants k_{ii} for both kernels versus the aggregate size in Fig. 6. For cluster sizes smaller than $i\cong 10$, both kernels are virtually identical. For larger aggregates, however, the Miyazima kernel starts to overestimate the aggregation rate constants with respect to the proposed kernel. Since the largest average chain lengths reported in this paper do not surpass the value of $i\cong 15$ (see Fig. 3), it is not surprising that both kernels lead to similar fits. According to the size dependence of both kernels, we expect the fits based on the Miyazima kernel to worsen for larger aggregates and longer aggregation times. Unfortunately, our experimental data do not reach out so far and so, we cannot unequivocally state that the Miyazima kernel cannot predict the long-time behavior of field induced aggregation processes. Hence, further investigation in this direction is needed before this question could be solved.

Finally, we would like to point out that the parameters in the Miyazima kernel have no clearly defined physical meaning. Especially, the meaning of the cross-sectional parameter C remains unclear. For the proposed kernel, however, the anisotropy of magnetic interaction as well as the long-range character of the net particle interaction are explicitly taken into account. Both characteristics are included on average in terms of the distinction between the attractive zone I and the repulsive zone II and the effective interaction range $\bar{h}$. In this sense, the proposed kernel may help to achieve a deeper insight in the kinetics of aggregating MF in presence of magnetic and electrostatic interactions.

V. CONCLUSIONS

In this work, the kinetics of magnetic filament formation was studied. Therefore, superparamagnetic particles were aggregated in the presence of a magnetic field at different electrolyte concentrations. The aggregation processes were monitored by means of dynamic light scattering.

Assuming the magnetic filaments to behave as cylindrical rodlike particles, the average filament length could be extracted from the experimental data. For this purpose, the effective diffusion coefficient had to be modelled considering mainly translational diffusive modes. The results obtained confirm that the average filament size increases monotonously with the exposure time to magnetic field. At fixed aggregation time, the filaments grow, on average, the larger the higher electrolyte concentration becomes. These results suggest that an effective control of the filament size might be achieved via an adequate manipulation of the relative strength of the isotropic electric and anisotropic magnetic interactions.

For all the experiments performed in this study, the length of the magnetic filaments was found to grow following an asymptotic power law with an electrolyte independent exponent of $z=0.67\pm0.04$. This means that the underlying aggregation mechanism is governed mainly by the anisotropic magnetic interactions. The isotropic electrostatic interactions, however, still show a strong influence on the growth kinetics. Furthermore, the time evolution of the average filament size could be rescaled such that the curves collapsed onto a single master curve. Using heuristic arguments, we proposed an aggregation kernel which takes into account the anisotropic character and the long range of the net particle interaction. The corresponding solutions of the Smoluchowski equation gave a very satisfactory description of the experimental data at all electrolyte concentrations even though only the effective range of the total interaction was left as a freely adjustable fit parameter.

ACKNOWLEDGMENTS

Financial support from the Spanish Ministerio de Educación y Ciencia (Plan Nacional de Investigación Científica, Desarrollo e Innovación Tecnológica (I+D+i), Contracts Nos. MAT2006-12918-C05-01 and MAT2006-13646-C03-03, the European Regional Development Fund (ERDF), and the Junta de Andalucía (Excellency Project FQM 392) are gratefully acknowledged. The authors also wish to express gratitude to Dr. Gerardo Odriozola for kindly providing the code of the stochastic method.

[1] A. M. Furst and A. P. Gast, Phys. Rev. E **62**, 6916 (2000).
[2] L. Cohen-Tannoudji, E. Bertrand, L. Bressy, C. Goubault, J. Baudry, J. Klein, J. F. Joanny, and J. Bibette, Phys. Rev. Lett. **94**, 038301 (2005).
[3] V. Cabuil, "Preparation and properties of magnetic nanoparticles," *Encyclopedia of Surface and Colloid Science* (Marcel Dekker, New York, 2004).
[4] R. Dreyfus, J. Baudry, M. L. Roper, M. Fermigier, H. A. Stone, and J. Bibette, Nature (London) **437**, 862 (2005).
[5] J. H. E. Promislow and A. P. Gast, J. Chem. Phys. **102**, 5942 (1995).
[6] S. Miyazima, P. Meakin, and F. Family, Phys. Rev. A **36**, 1421 (1987).
[7] S. Relle, S. B. Grant, and C. Tsouris, Physica A **270**, 427 (1999).
[8] M. Carmen Miguel and R. Pastor-Satorras, Phys. Rev. E **59**, 826 (1999).
[9] S. Melle, M. A. Rubio, and G. G. Fuller, Phys. Rev. Lett. **87**, 115501 (2001).
[10] S. Fraden, A. J. Hurd, and R. B. Meyer, Phys. Rev. Lett. **63**, 2373 (1989).
[11] T. Maeda and S. Fujime, Macromolecules **17**, 1157 (1984).
[12] F. Martínez Pedrero, M. Tirado Miranda, A. Schmitt, and J. Callejas Fernández, J. Chem. Phys. **125**, 084706 (2006).
[13] M. Tirado and J. García de la Torre, J. Chem. Phys. **71**, 2581 (1979).
[14] M. Y. Lin, H. M. Lindsay, D. A. Weitz, R. Klein, R. C. Ball, and P. Meakin, J. Phys.: Condens. Matter **2**, 3093 (1990).
[15] M. Y. Lin, H. M. Lindsay, D. A. Weitz, R. C. Ball, R. Klein, and P. Meakin, Phys. Rev. A **41**, 2005 (1990).
[16] T. Vicsek, *Fractal Growth Phenomena* (World Scientific, Singapore, 1992).
[17] H. C. van de Hulst, *Light Scattering by Small Particles* (Dover, New York, 1981).
[18] M. von Smoluchowski, Z. Phys. Chem., Stoechiom. Verwandtschaftsl. **92**, 129 (1917).
[19] H. Sonntag and K. Strenge, *Coagulation Kinetics and Structure Formation* (Plenum, New York, 1987).
[20] S. Cutillas and J. Liu, Phys. Rev. E **64**, 011506 (2001).
[21] G. Odriozola, A. Schmitt, J. Callejas-Fernández, R. Martínez-García, and R. Hidalgo-Alvarez, J. Chem. Phys. **111**, 7657 (1999).